

Characterization of red fluorescent reporters for dual-color *in vivo* three-photon microscopy

Michael A. Thornton,^{a,b} Gregory L. Futia,^c Michael E. Stockton,^{a,b}
Baris N. Ozbay,^d Karl Kilborn,^d Diego Restrepo,^{a,b}
Emily A. Gibson^{b,c,*} and Ethan G. Hughes^{a,b,*}

^aUniversity of Colorado Anschutz Medical Campus, Department of Cell and Developmental Biology, Aurora, Colorado, United States

^bUniversity of Colorado Anschutz Medical Campus, Neuroscience Program, Aurora, Colorado, United States

^cUniversity of Colorado Anschutz Medical Campus, Department of Bioengineering, Aurora, Colorado, United States

^dIntelligent Imaging Innovations (3i), Denver, Colorado, United States

Abstract

Significance: Three-photon (3P) microscopy significantly increases the depth and resolution of *in vivo* imaging due to decreased scattering and nonlinear optical sectioning. Simultaneous excitation of multiple fluorescent proteins is essential to studying multicellular interactions and dynamics in the intact brain.

Aim: We characterized the excitation laser pulses at a range of wavelengths for 3P microscopy, and then explored the application of tdTomato or mScarlet and EGFP for dual-color single-excitation structural 3P imaging deep in the living mouse brain.

Approach: We used frequency-resolved optical gating to measure the spectral intensity, phase, and retrieved pulse widths at a range of wavelengths. Then, we performed *in vivo* single wavelength-excitation 3P imaging in the 1225- to 1360-nm range deep in the mouse cerebral cortex to evaluate the performance of tdTomato or mScarlet in combination with EGFP.

Results: We find that tdTomato and mScarlet, expressed in oligodendrocytes and neurons respectively, have a high signal-to-background ratio in the 1300- to 1360-nm range, consistent with enhanced 3P cross-sections.

Conclusions: These results suggest that a single excitation wavelength source is advantageous for multiple applications of dual-color brain imaging and highlight the importance of empirical characterization of individual fluorophores for 3P microscopy.

© The Authors. Published by SPIE under a Creative Commons Attribution 4.0 International License. Distribution or reproduction of this work in whole or in part requires full attribution of the original publication, including its DOI. [DOI: [10.1117/1.NPh.9.3.031912](https://doi.org/10.1117/1.NPh.9.3.031912)]

Keywords: multiphoton microscopy; glia-neuron interactions; fluorescent proteins.

Paper 21058SSR received Oct. 19, 2021; accepted for publication Mar. 23, 2022; published online Apr. 28, 2022.

1 Introduction

Multiphoton microscopy methods allow for high-resolution structural and functional imaging deep into biological tissues.¹⁻³ Two-photon (2P) microscopy is a widely used technique to assess cellular and subcellular dynamics in the intact mouse brain. Although multiple excitation source 2P microscopy setups are increasingly common,^{4,5} broad excitation profiles of specific green and red fluorescent proteins allow simultaneous dual-color 2P imaging using a single tunable excitation source.⁶ This single-wavelength excitation dual-color 2P microscopy approach has benefited from careful characterizations of fluorescent protein excitation

*Address all correspondence to Emily A. Gibson, emily.gibson@cuanschutz.edu; Ethan G. Hughes, ethan.hughes@cuanschutz.edu

cross-sections at relevant wavelengths^{7–9} and enabled both functional and structural interrogation of neural dynamics *in vivo*. For example, simultaneous 1000 nm excitation of GCaMP6s/jRGECO1a permitted the detection of correlated axonal and dendritic calcium events in the visual cortex,¹⁰ while 920 nm excitation of enhanced green fluorescent protein (EGFP)/tdtomato was used to track oligodendroglial differentiation and cell fate over time.¹¹ However, *in vivo* dual-color 2P microscopy is practically limited in imaging depth to the superficial mouse cortex by light scattering and the generation of out-of-focus background.

The development of three-photon (3P) microscopy, which utilizes low rep-rate, high pulse energy excitation sources at 1300 to 1700 nm, has significantly improved imaging depth and resolution due to decreased scattering and improved signal-to-background ratio (SBR).^{3,12} Note that 3P microscopy with 1700 nm excitation was first used in the intact mouse brain to image cortical and subcortical vasculature as well as red fluorescent protein (RFP)-labeled neurons throughout the visual cortex, cortical subplate, and hippocampus.¹² Since then, 1300 nm excitation of GCaMP6s has been used to record spontaneous neuronal activity throughout the cortical-subcortical volume¹³ and the sensitivity of these recordings and concomitant thermal and phototoxic changes have been characterized extensively.¹⁴ Simultaneous dual-color *in vivo* 3P microscopy remains challenging due to the large spectral separation in the optimal wavelength excitation windows for GFPs and RFPs, centered at 1300 and 1700 nm,^{3,12} which currently necessitate independent dispersion compensation and custom optical elements with increased 1700 nm transmission.

Dual-color 3P microscopy of green and red fluorescent indicators was achieved in the fixed mouse brain using a unique two-stage optical parametric chirped-pulse amplifier seeded by a Ytterbium-doped fiber amplifier¹⁵ for 1300 and 1700 nm simultaneous output. However, issues associated with the overlap of the two wavelengths at the focus and the requirement of higher powers ($\sim 1 \mu\text{J}$) prohibit the application of this method to *in vivo* imaging in the mouse brain.^{14,16} Alternatively, a recent report showed that single-wavelength 1300 nm excitation can be used with compatible combinations of fluorophores to achieve deep tissue simultaneous dual-color imaging in the living mouse brain via higher-energy electronic excited states of the fluorophores.¹⁷ However, a lack of information on the 3P excitation properties of commonly used fluorophores currently limits the broad application of this approach. Here, we characterize the use of two RFPs with potentially enhanced excitation properties for *in vivo* single-source excitation 3P microscopy. The results obtained by utilizing this method to perform cell fate tracking, cell localization for holographic stimulation, and subcellular neuronal and glial imaging deep in the living mouse brain will be important for future studies.

2 Methods

2.1 Animals

Animal experiments were conducted in accordance with protocols approved by the Animal Care and Use Committee at the University of Colorado Anschutz Medical Campus. Male and female mice used in these experiments were kept on a 14-h light to 10-h dark schedule with ad libitum access to food and water and were housed with littermates. C57BL/6N *MOBP-EGFP* (MGI:4847238), *Olig2tm1(cre/Esr1*)Htak* (MGI:2183410), and *B6.Cg-Gt(ROSA)26Sortm9(CAG-tdTomato)Hze/J* (JAX #007909) were used for dual-color 3P imaging. Generation and genotyping of mice were performed as described previously.¹¹

2.2 Custom 3P Microscope

A VIVO Multiphoton Open (3i) microscope, based on a Sutter Moveable Objective Microscope, was modified for 3P imaging. The excitation source was a regenerative amplifier with 1030 nm center wavelength, 70 W average power, <300 fs pulse duration, adjustable repetition rate up to 2 MHz (Spirit-1030-70, Spectra Physics), wavelength converted by a non-collinear optical parametric amplifier (NOPA-VIS-IR, Spectra Physics). The idler output of the NOPA is tunable in

the range of 1200 to 2500 nm. The laser was operated at a repetition rate of 1 MHz and the final output power from the idler was 0.8 to 1.1 W at 1300 nm. The power was modulated with a motorized half-wave plate (KPRM1E/M - Ø1, Thorlabs). Beam conditioning of the NOPA output consisted of a Glan-Thompson prism, an expansion and collimating lens relay ($f_1 = 75$ mm, $f_2 = 100$ mm, Newport), a 4× reflective beam expansion telescope (BE04R, Thorlabs), and a beam demagnifying telescope ($f_1 = 500$ mm, $f_2 = 200$ mm, Edmund Optics). The additional reflective beam expansion telescope and de-magnification were to condition the beam size for a deformable mirror that was held flat for this study. Group delay dispersion (GDD) compensation was achieved using a prism compressor system consisting of two 25 mm SF10 prisms cut at Brewster's angle (10NSF10, Newport), and a gold roof mirror (HRS1015-M01, Thorlabs). The beam was directed to the galvanometers (Cambridge Technologies) and through a scan lens (Thorlabs SL50-3P), tube lens, and a 760 nm long-pass primary dichroic. The back aperture of a high-NA multiphoton objective (XLPLN25XWMP2, 25x/1.05 NA, Olympus) was ~75% filled for 3P imaging. The fluorescent emission was separated from the excitation path by the long pass dichroic mirror and spectrally filtered (green channel = 525/50 nm, red channel = 620/60 nm), and detected by photomultiplier tubes (H10770PA-40, Hamamatsu). The electronic signal was amplified, low-pass filtered and digitized. Data were acquired with SlideBook 2021 (Intelligent Imaging Innovations).

2.3 2P Microscopy

2P images in Fig. S2 in the [Supplemental Materials](#) were generated using a wavelength-tunable femtosecond oscillator (MaiTai-HP DeepSee, Spectra Physics) combined with the 3P excitation path with a 1030 nm long-pass filter after the prism compressor and aligned to co-propagate with the 1300 nm light.

2.4 GDD Tuning and Pulse Measurements

To tune the prism compressor for optimizing 3P excitation, we performed time-lapse imaging of a green fluorescent flat slide and adjusted the prism separation and insertion in real-time to maximize the fluorescent signal. We checked but did not need to make any changes in the compressor for maximum signal over multiple months of imaging. Pulse measurements were made using frequency-resolved optical gating (FROG) (FROGscan, Mesa Photonics). The FROG has an all-reflective optical path from its input to the Beta Barium Borate crystal used for second-harmonic generation (SHG) to avoid adding any additional dispersion. For the same reason, a reflective objective of $40\times/0.5$ NA (LMM40X-UVV, ThorLabs) was used to collimate the beam after focusing through the objective, immersion water, and coverglass, followed by two silver mirrors to align into the FROG. This setup allowed us to characterize our pulse duration at the sample without additional dispersive elements that would change our pulse profile. We characterized the pulses for all wavelengths (Fig. 1, 1225 to 1360 nm). For the 2P excitation, we used the internal GDD tuning on the MaiTai-HP DeepSee to find the maximum signal intensity at each wavelength.

2.5 Stereotaxic Adeno-Associated Virus (AAV) Injections

Six- to eight-week-old mice were anesthetized with isoflurane inhalation (induction, 5%; maintenance, 1.5% to 2.0%, mixed with 0.5 L/min O₂) and kept at 37°C body temperature with a thermostat-controlled heating plate. A midline incision in the skin was made with fine surgical scissors to expose the skull. A small burr hole was made with a high-speed dental drill over the right forelimb primary motor cortex (1 mm anterior and 1.5 mm lateral to Bregma) and the deep layer of the thinned skull was removed with a curved 27-gauge needle. To label layer V/VI cortical neurons, we made two 500 nL injections of AAV8-hSyn-mScarlet-WPRE¹⁸ (1.5×10^{12} vg/mL, Deisseroth Lab, Stanford Viral Vector Core) at 1000 and 750 μ m depths below the pial surface at a rate of 100 nL/min. The injection needle was left in place for 5 min to prevent backflow and then removed slowly. The burr hole was filled with Vetbond (3M) and the skin incision was sutured using 5-0 Ethilon sutures.

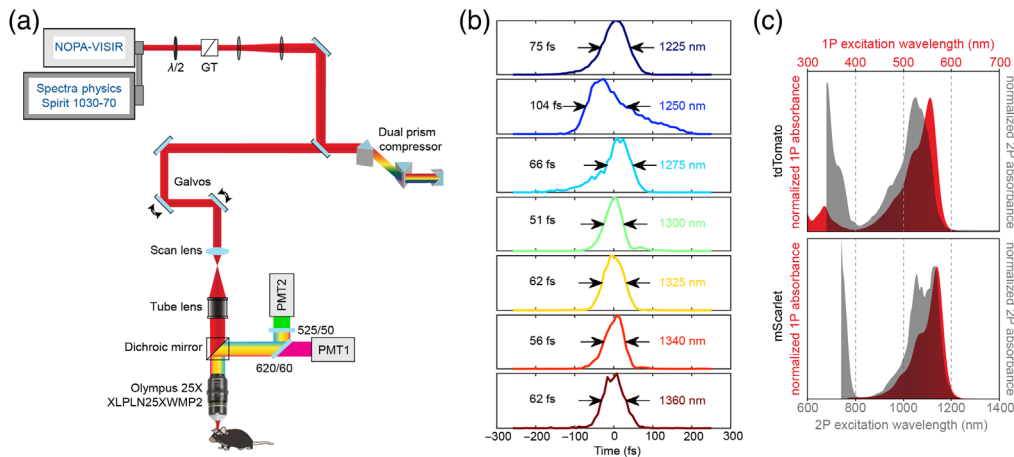


Fig. 1 Custom 3P microscope for dual-color *in vivo* imaging. (a) 3P light path and detection scheme for dual-color imaging. (b) Laser pulse temporal profile for wavelengths from 1200 to 1400 nm, using FROG. Pulses were characterized by the objective focus. Pulse widths indicated are the full width at half maximum (FWHM). (c) 1P and 2P excitation curves for tdTomato and mScarlet, recreated from FPbase. Note the small tdTomato excitation peak in the UV and the short wavelength 2P excitation peaks in the range of 750 to 800 nm.

2.6 In Vivo Multiphoton Microscopy

Cranial windows were prepared as previously described.¹⁹ Six- to 10-week-old mice were anesthetized and monitored as above. After removal of the skin over the right cerebral hemisphere, the skull was cleaned and a 2 mm × 2 mm region of the skull centered over either (a) the posterior parietal cortex (PPC) (−1 to −3 mm posterior to bregma and 1 to 3 mm lateral), or (b) the forelimb region of the primary motor cortex (0 to 2 mm anterior to bregma and 0.5 to 2.5 mm lateral) was removed using a high-speed dental drill. A piece of the cover glass (VWR, No. 1) was placed in the craniotomy and sealed with Vetbond (3M), and then secured with dental cement (C&B Metabond). A 5 mg/kg dose of carprofen was subcutaneously administered before awakening and for three additional days for analgesia. For head stabilization, a custom metal plate with a 6 mm central hole was attached to the skull. The headbar was secured very close to the skull to enable deep 3P imaging without the steric hindrance of the objective. Custom three-dimensional (3D)-printed headbar holders (CU Anschutz Optogenetics and Neural Engineering Core) were attached to a 200-mm breadboard (Thorlabs) affixed to stacked dual-axis goniometers (Optosigma, ±15°, GOH-65B76R) such that the rotation center height was located at the headbar. Before imaging, the angle of the cranial window was adjusted to be perpendicular to the axis of the excitation beam using the goniometers.

In vivo imaging measurements were taken either immediately following the surgery (acute preparation) or 2 to 3 weeks post-surgery (chronic preparation) as noted in the figures. During imaging sessions, mice were anesthetized with isoflurane and immobilized by attaching the head plate to the custom stage, and the temperature was monitored continuously as above. Images were acquired using Slidebook 2021 (3i) imaging software with three key modifications to standard laser point scanning systems for 3P imaging: (1) the laser was blanked during the galvanometer overscan to reduce the average power at the sample outside of the imaging field of view (FOV), (2) Slidebook 2021 was modified to allow for fine power control of the motorized half-wave plate (±0.1%), and (3) scanning was intermittently paused for 1 min after every 3 min of continuous scanning to allow for heat dissipation.²⁰ Large 3D structural *z* stacks were acquired at 512 × 512 pixels, 2 μs dwell time, and frame averaging = 2, with a FOV of 385 μm × 385 μm with a 3 μm *z*-step. *Z*-stacks for optical measurements were acquired with the same settings without frame averaging and with a 0.5 μm *z*-step. The power after the objective was measured daily by centering the galvanometers and acquiring a point-scan power curve on a high-power microscope slide meter sensor head (S175C, Thorlabs) in immersion water. The maximum power at the sample was 1 to 55 mW (0 to 1100 μm depth).

2.7 Image Processing and Analysis

Image stacks were registered with StackReg²¹ before analysis with ImageJ.²² All images shown are either raw or filtered with a 0.5 μm median filter, as noted in the figure legends. Z-width of max projected images is also noted in the figures. SBR analysis was performed using ImageJ on 3 to 10 cells located $\pm 5 \mu\text{m}$ from the indicated depth. For each wavelength and pulse energy measured, a z-stack was acquired, an region of interest (ROI) was drawn over the cell body of interest, and the Plot z axis Profile ImageJ command was used to find the z-plane of peak intensity. All measurements were made at this single plane image. For the peak signal, a line scan was made through the cell body and the five-pixel values surrounding the maximum were averaged. For SBR measurements of mScarlet, the background fluorescence was measured within the area of an unlabeled neuron to avoid measuring virally labeled neurites as background fluorescence. Plotting and statistical analyses were performed in JMP 15 (SAS). SBR measurements were expressed as mean (SD). Logarithmic pulse Fig. 3(c) energy versus signal plots [Fig. 3(c) and Figs. S3 and S4 in the [Supplemental Materials](#)] were analyzed using linear regression (MSE, mean square error) and the slopes were expressed as mean \pm SEM. The pulse energy at the focal plane (z-depth) in Fig. S2 in the [Supplemental Materials](#) and in Fig. 4 was calculated with the equation below, using a linear extrapolation of previously published experimental effective attenuation lengths (EALs) in the mouse neocortex,^{12,14,23} where P = average power, f = laser repetition rate (1 MHz), and z = cortical depth and the related equation is given by

$$(P/f)_{\text{focal plane}} = (P/f)_{\text{surface}} * e^{-\left(\frac{z}{\text{EAL}}\right)}.$$

3 Results

3.1 Frequency-Resolved Optical Gating Pulse Measurements

To overcome the fundamental depth limit of 2P imaging in the mouse brain,²⁴ we built a custom 3P microscope with a multichannel emission detection path [Fig. 1(a)]. With the ultimate goal of measuring the *in vivo* excitation properties of RFPs for simultaneous dual-color 3P microscopy, we first characterized our output pulses after the objective at a range of wavelengths using FROG.²⁵ Pulse characterization with FROG allows for the recovery of spectral intensity and phase using iterative spectrogram inversion algorithms and provides a ground-truth pulse width measurement.^{26,27} We optimized the prism pulse compressor at 1300 nm to achieve 51 fs pulses and a pulse duration of 51 to 75 fs for 1225 to 1360 nm, except for 1250 nm, which was 104 fs [Fig. 1(b)]. The raw spectrograms, retrieved spectral intensities, phases, and third-order fit GDD and third-order dispersion magnitudes are presented in Fig. S1 in the [Supplemental Materials](#). The prism compressor was optimized at 1300 nm and maintained at the same settings for all measurements. The one-photon (1P) and 2P excitation peaks for tdTomato are 554 and 1050 nm, while mScarlet is maximally excited at 569 nm and has a bimodal 2P excitation curve with peaks at 1065 and 1143 nm [Fig. 1(c)].^{9,28-32}

3.2 Nonlinear Excitation Properties of tdTomato in the Living Mouse Brain at Depth

We implanted chronic cranial windows over the PPC of triple transgenic mice (*Olig2-CreER*; *RCL-tdTomato*; *MOBP-EGFP*, OTM) that express tdTomato in oligodendrocyte lineage cells and EGFP specifically in mature oligodendrocytes and myelin sheaths.¹¹ Single-excitation structural 3P microscopy of the brain volumes from OTM mice revealed single- and dual-labeled oligodendrocyte lineage cells throughout the cortical layers and subcortical white matter [Figs. 2(a) and 2(b)]. To maintain constant average power at the brain surface, the laser power after the objective was measured at each wavelength and adjusted before imaging. We found that the pulse energies required for imaging were similar to those recently published for structural and functional neuronal imaging *in vivo*, and importantly, below the limits for heating- and nonlinear absorption-induced damage.^{14,16,33} To determine the *in vivo* 3P excitation properties of tdTomato, we measured the fluorescent signal, background, and SBR in layer 6b of the PPC (760 μm

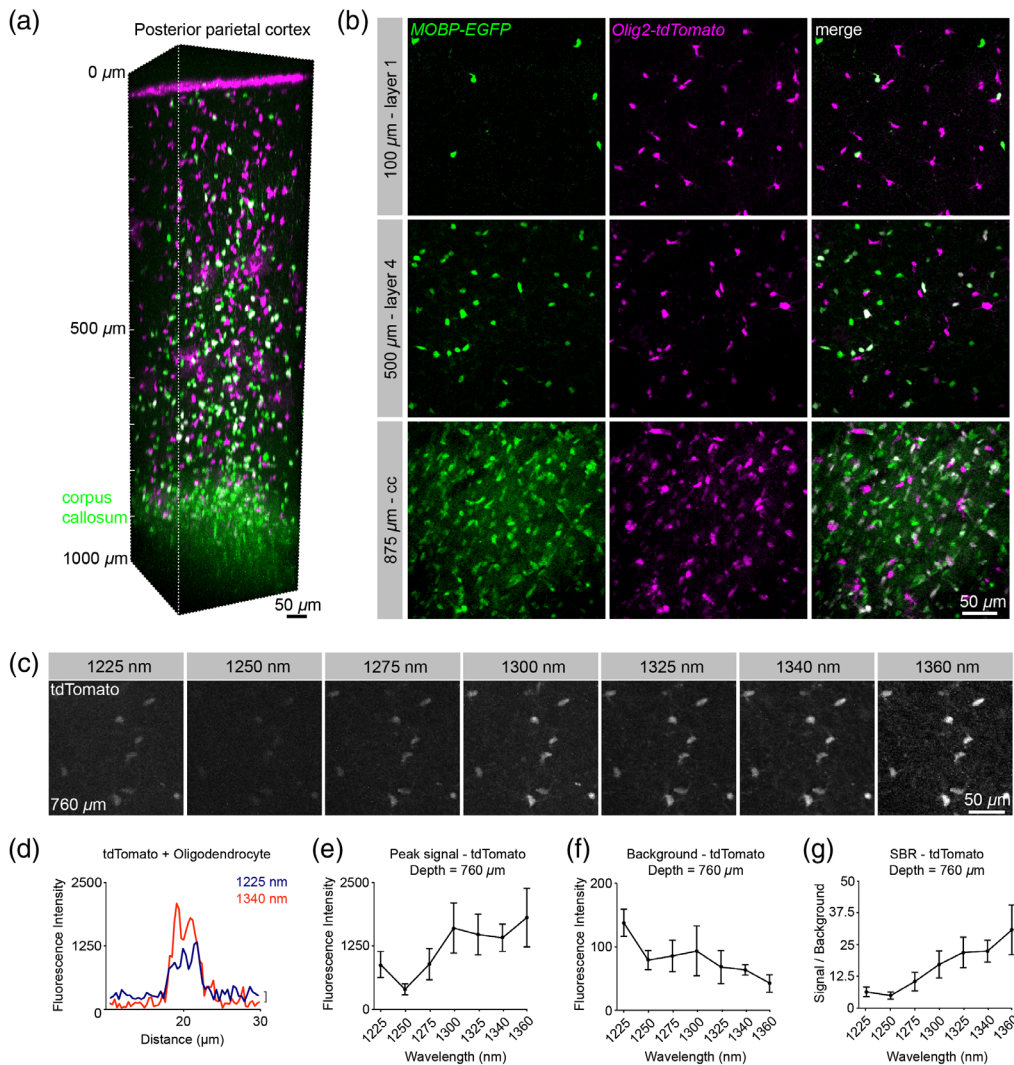


Fig. 2 Simultaneous 3P excitation of EGFP and tdTomato in PPC. (a) 3D image volume from a chronic implanted cranial window in an *Olig2-CreER; RCL-tdTomato; MOBP-EGFP* mouse at P60. (b) Max projections of $\sim 50 \mu\text{m}$ volumes in cortical layers 1 (top), 4 (middle), and the corpus callosum (cc, bottom). Note the highly myelinated corpus callosum shows an increased density of dual-labeled mature oligodendrocyte cell bodies and strong *MOBP-EGFP* myelin signal compared to the superficial cortex. (c) Max projection images of 9 μm volumes at 760 μm depth and a range of excitation wavelengths with average power = 45.2 mW. (d) Example line scan plots through a single tdTomato-positive oligodendrocyte cell body at 1225 and 1340 nm show increased signal and decreased background with longer wavelength excitation. (e) Max fluorescence signal of tdTomato-positive oligodendrocyte lineage cells. (f) Background fluorescence in the tdTomato detection channel. (g) Signal to background ratio versus wavelength comparison of the tdTomato signal at 760 μm depth (e–g) Plots include measurements taken with average power = 45.2 mW after the objective and pulse energy = ~ 2.5 to 3.6 nJ at the focus. Data represent $n = 10$ cells from a triple transgenic mouse and are represented as the mean \pm standard deviation. Due to low output power at 1360 nm, the data at this wavelength were acquired using 36 mW after the objective and then scaled by a value of $1.98 = (45.2/36.0)^3$.

depth) of tdTomato at a range of wavelengths (1225 to 1360 nm) and constant average power at the surface [Figs. 2(c)–2(g)]. The peak signal increased at 1300 versus 1225 and 1250 nm (mean (SD) = 1606.98 (499.02) versus 879.66 (260.38), 386.79 (110.631), respectively), and plateaued through 1360 nm [Fig. 2(e)], consistent with a broad excitation range for tdTomato in the 1300-nm range. However, we found that the background decreased from 1300 to 1360 nm, resulting in an increased SBR in the 1325- to 1360-nm range when compared to 1300 nm [Fig. 2(g),

21.91 (6.01), 22.39 (4.32), 30.74 (9.78) versus 17.13 (5.32), respectively]. To assess the contribution of 2P versus 3P excitation processes to signal generation for each wavelength, we generated logarithmic signal versus pulse energy plots at each wavelength for a range of pulse energies at the focal plane (2.3 to 3.8 nJ, Fig. S2 in the [Supplemental Materials](#)). The slope of the logarithmic plot for tdTomato at 1225 nm was 2.171 ± 0.526 , indicating a larger contribution of 2P than 3P excitation to the fluorescent emission at this wavelength and imaging depth. The log-plot slopes at 1300 and 1325 nm were 3.066 ± 0.390 and 2.874 ± 0.369 , respectively, indicating that 3P excitation dominates in the 1300-nm range for tdTomato. These *in vivo* results are consistent with recently published 2P and 3P action cross-sections of purified samples.¹⁷ Our data indicate that the significant decrease in out-of-focus (2P) background with longer-wavelength 3P excitation of tdTomato drives the observed increase in the SBR of this fluorophore.

3.3 Nonlinear Excitation Properties of mScarlet in the Living Mouse Brain at Depth

Historically, limitations in the maturation and quantum yield of monomeric RFPs have hampered their usage. Recently, a truly monomeric protein with high brightness and quantum yield, mScarlet, was developed.³⁴ This fluorophore has been included in a unique suite of viral tools used to express the highly sensitive, red-shifted opsin, ChRmine, to provide a red-shifted fluorescent reporter for structural imaging of targeted cells and subcellular structures.¹⁸ To investigate the utility of mScarlet for dual-color 3P microscopy, we injected AAV8-hSyn-mScarlet-WPRE into the deep layers of the primary motor cortex to label motor output neurons. These injections were performed in *MOBP-EGFP* mice, which express EGFP in myelinating oligodendrocytes, to allow visualization of neuron-glia interactions. Single-excitation structural 3P microscopy of mScarlet-injected *MOBP-EGFP* mice permitted the simultaneous visualization of excitatory neurons and mature oligodendrocytes at depths up to 1100 μm in the forelimb motor cortex [Fig. 3(a)]. Large diameter layer 5/6 neuronal cell bodies were labeled at depths greater than 800 μm and mScarlet-positive processes were labeled throughout the cortical volume [Figs. 3(a) and 3(b)]. To characterize the 2P excitation profile of mScarlet, we measured the *in vivo* 2P SBR of mScarlet at a range of wavelengths centered at 950 nm at a depth of 400 μm from the brain surface. We found that the *in vivo* SBR of the two fluorophores intersected at ~ 960 nm suggesting that this may be an ideal wavelength for 2P dual-color imaging of EGFP and mScarlet (Fig. S3 in the [Supplemental Materials](#)). However, we found an acceptable dual-color cellular signal was achieved from 920 to 1000 nm, highlighting the broad applicability of this fluorophore combination at wavelengths with sufficient output power from standard multiphoton lasers. These *in vivo* 2P excitation data build upon recently published mScarlet cross-section results in a solution showing a bimodal excitation curve with an initial peak near 1060 nm [Fig. 1(c)].²⁹ Next, we measured the 3P SBR of mScarlet in the deep primary motor cortex (920 μm below the brain surface) at a range of excitation wavelengths and constant average power at the surface. We found that mScarlet showed a large signal increase at 1225 nm yet had a high out-of-focus background that substantially reduced the SBR at this wavelength [Figs. 3(c)–3(f)], likely due to the predominance of 2P over 3P excitation at shorter wavelengths. While the mScarlet signal initially decreased from 1250 to 1275, it subsequently increased from 1300 to 1360 nm [Fig. 3(d)]. Unexpectedly, we found that the mScarlet background plateaued from 1300 to 1360 nm, despite choosing ROIs within unlabeled neuronal shadows. However, these *in vivo* measurements may still overestimate the background at longer wavelengths due to strong diffuse labeling in the AAV-injected mice [Figs. 3(c) and 3(e)]. The mean mScarlet SBR plateaued from 1340 to 1360 nm, which may represent an excitation peak for higher-order excitation in the 1300-nm range [Fig. 3(f)]. To determine the contributions of 2P versus 3P excitation we generated logarithmic signal versus pulse energy plots at each wavelength for mScarlet as above (Fig. S4 in the [Supplemental Materials](#)). We found that the slope of the logarithmic mScarlet plot at 1225 nm was 1.885 ± 0.896 , reflecting the strong contribution of 2P excitation at this wavelength [Fig. S4 in the [Supplemental Materials](#) and Figs. 3(c) and 3(d)]. In contrast, we found that the slope at 1340 nm was 2.915 ± 2.05 , confirming the predominant contribution of 3P excitation at wavelengths greater than 1325 nm for mScarlet (Fig. S4 in the [Supplemental Materials](#)). Together, our data suggest that mScarlet is an attractive RFP with an enhanced 3P

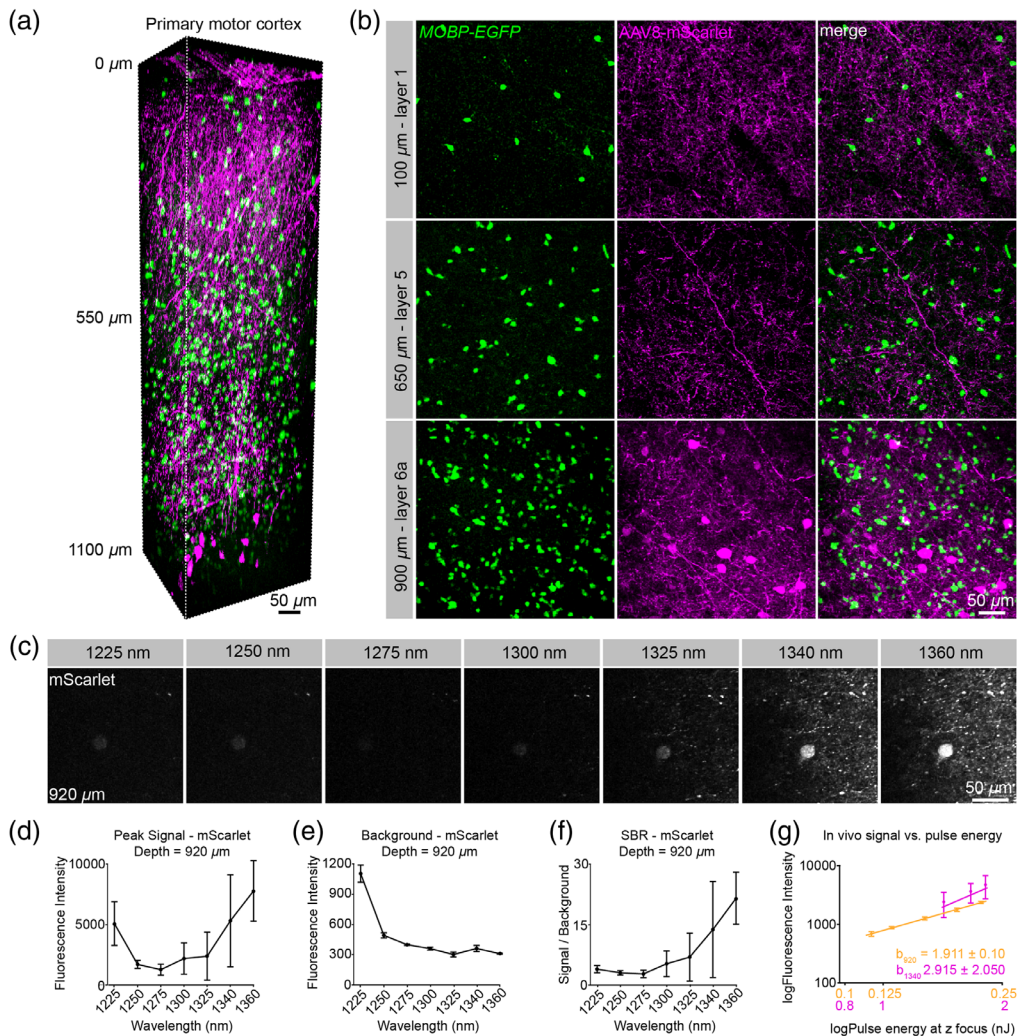


Fig. 3 Simultaneous 3P excitation of EGFP and mScarlet in the primary motor cortex. (a) 3D image volume from an acutely implanted cranial window in an *MOBP-EGFP* mouse at P65 that was injected with AAV8-hsyn-mScarlet virus at 1000 and 750 μm depths in the primary motor cortex. Note large mScarlet-positive layer 5/6 motor output neurons are labeled at the bottom of the image volume and neuronal processes of these cells are labeled throughout the volume. (b) Max projection images of $\sim 30 \mu\text{m}$ volumes in cortical layers 1 (top), 5 (middle), and 6a (bottom). (c) Max projection images of 9 μm z-width at 920 μm depth show differences in signal and background fluorescence across a range of excitation wavelengths. Note the increased signal and background at 1225 nm. (d) Max fluorescence signal of mScarlet-positive neurons for the range of wavelengths. (e) Background fluorescence measurements in the mScarlet channel. (f) Signal to background ratio versus wavelength comparison of mScarlet signal at a depth of 920 μm from the brain surface. (g) log-log signal versus pulse energy plots illustrate the contribution of 2P and 3P excitation to the fluorescence intensity for mScarlet at 920 (orange) and 1340 nm (magenta). The steeper slope of the 1340 nm line plots indicates a greater contribution of 3P excitation to the signal at the longer wavelength (theoretical 3P/2P ratio = 1.5). d-g) plots include measurements taken with average power = 47.7 mW after the objective and pulse energy = ~ 1.3 to 2 nJ at the focus. Data represent $n = 3$ labeled neurons from a virally injected transgenic mouse and are represented as the mean \pm standard deviation. Due to low output power at 1360 nm, the data at this wavelength were acquired using 38.5 mW after the objective and then scaled by a value of $1.90 = (47.7/38.5)^3$.

cross-section in the 1300-nm range for use in single excitation source dual-color *in vivo* 3P imaging experiments.

3.4 Modeling of the Excitation Probability and Brain Heating for tdTomato in the 1300- to 1650-nm Range

Simultaneous dual-color 3P excitation in the 1300-nm range may require the excitation of fluorophores at sub-optimal excitation wavelengths, resulting in increased excitation power and heating. To model the probability of excitation for tdTomato we used 3P action cross-section data¹⁷ and infrared water absorption values³⁵ in the equation, which is stated as¹⁴

$$\text{Pr} = 1 - \exp \left[-\frac{g_p^{(3)}}{\tau^2} \sigma_3 \left(\frac{\text{NA}^2 \pi}{\lambda_{3p}^2} \right)^3 \left(\frac{P_{3p}}{f} \right)^3 \right],$$

where $g_p^{(3)}$ = third-order temporal coherence factor, τ = pulse duration (s), σ_3 = 3P cross-section, NA = objective numerical aperture, λ = excitation wavelength, P_{3p} = photons/s at the focal plane, and f = laser repetition rate. The modeled probabilities of excitation for 1300, 1340, and 1650 nm are presented in Fig. S5a in the [Supplemental Materials](#) and the power at the surface values required for 10% excitation probability per pulse are presented in Fig. S5b in the [Supplemental Materials](#). With 30 mW at the surface and $z = 800 \mu\text{m}$, the excitation probability per pulse are .07, .11, and .26 for 1300, 1340, and 1650 nm, respectively. Therefore, a 10% excitation probability is achieved with 34.5, 29, and 21 mW average power at the surface for 1300, 1340, and 1650 nm, respectively, for the specific parameters of our microscope. The water absorption coefficient at 1300 nm is ~22% of that at 1650 nm (0.136 versus 0.616 mm^{-1}).³⁵ Because heating scales nearly linearly with input power¹⁴ optimal excitation versus heating is achieved in the 1300-nm range. Additionally, the 3P action cross-section for tdTomato is slightly greater at 1320 nm than at 1340 nm (3.3 versus $3.13 \times 10^{-82} \text{ cm}^6 (\text{s/photon})^2$),¹⁷ which is in agreement with our *in vivo* SBR values [Fig. 2(g)]. Therefore, ~1320 nm is the optimal excitation wavelength for single-wavelength 3P excitation of EGFP and tdTomato. Our *in vivo* SBR measurements for mScarlet [Fig. 3(f)] suggest that the optimal excitation wavelength will be slightly red-shifted from tdTomato, however future 3P action cross-section experiments for mScarlet, combined with empirical fine-tuning of excitation parameters will be essential in determining these values for *in vivo* imaging.

4 Discussion

4.1 tdTomato and mScarlet Have Enhanced 3P Cross-Sections in the 1250- to 1350-nm Range

A recent study showed that while excitation in the 1600- to 1700-nm range resulted in appreciable 3P excitation to the lowest energy state, certain RFPs have an order of magnitude larger 3P action cross-section in the 1260- to 1360-nm range.¹⁷ Here, we took advantage of these 3P excitation properties to characterize the *in vivo* behavior of a classical tandem dimer RFP (tdTomato), as well as a recently developed monomeric RFP (mScarlet), for use in simultaneous dual-color 3P imaging studies. We found that both tdTomato and mScarlet have favorable 3P excitation properties in the 1300- to 1340-nm range and we empirically defined the optimal excitation wavelengths for the best SBR at depth, which will be applicable to future dual-color *in vivo* imaging experiments. Similar to Hontani et al.¹⁷ we found that tdTomato exhibited a broad 3P excitation curve that increases significantly from 1250 to 1300 nm and plateaus through 1360 nm. We found that the improvement in the SBR at the longer wavelengths (1300 to 1360 nm) was largely due to decreased out-of-focus background generation at these wavelengths. In contrast, the signal versus wavelength curve for mScarlet was slightly red-shifted, as the peak signal increased significantly from 1325- to 1360-nm wavelengths; however, mScarlet also showed exceptional signal to background in this range. These results suggest that both of these red fluorophores have advantageous excitation properties in the short 3P wavelength range (1300 to 1340 nm). Future characterization of additional red fluorophores in the

1300- to 1700-nm range will be useful to direct the application of both structural and functional *in vivo* dual-color 3P imaging.

4.2 1300 to 1360 nm Excitation of RFPs Likely Represents Excitation to a Higher Energy Molecular State

Certain red fluorescent proteins like Texas Red, tdTomato, and mScarlet exhibit short-wavelength 1P absorption bands (~400 to 450 nm) that represent excitation to higher-energy electronic states. Multiphoton excitation wavelengths used with classically employed fluorescent indicators likely induce excitation to the lowest-energy excited state (absorption peak), which has empirically generated optimal signal to noise in 2P experiments (e.g., 1040 nm excitation of tdTomato). However, our current findings suggest that 3P excitation is enhanced in these lower-wavelength absorption bands and has considerable implications for the design and implementation of future dual-color 3P studies. In addition, the ~1260- to 1340-nm range of 3P excitation wavelengths overlaps with the long-wavelength tail of the 2P absorption cross-section for most RFPs, therefore, the signal detected at wavelengths less than ~1300 nm represents a mix of 2P and 3P excitation. We found that the mScarlet signal detected at 1225 nm was greater than in the 1250- to 1325-nm range, likely due to the low energy tail in the mScarlet 2P absorption cross-section curve. However, consistent with 2P excitation dominating at this wavelength, we measured high out-of-focus background generation at 1225 nm which severely decreases contrast and SBR at increased depths.

4.3 Complete Characterization of Laser Pulses for 3P Excitation in the 1200 to 1360 nm Wavelength Range

We used FROG to measure the electric field of our laser pulses at the different wavelengths for 3P microscopy. Previously, autocorrelation measurements in the 1200- to 1400-nm range have been presented.^{12,17} FROG measurements have an advantage over autocorrelation in that both the intensity and phase of the pulse can be retrieved from the spectrograms and is useful for pulses with complex temporal profiles.²⁶ The retrieval of the electric field is done without prior assumptions of pulse shape, which are required for estimating pulse widths from autocorrelation measurements. Calculation of the time-bandwidth product and the spectral phase can determine whether the pulse is optimally temporally compressed at the sample. While there are a variety of FROG instrument geometries,²⁶ we used SHG-FROG. One limitation of SHG-FROG is that the direction of time of the pulse is not captured in the measurement.^{36,37} This makes time-reversed traces in Fig. 1 equally likely and leads to ambiguity in the sign of the spectral phase. We measured an asymmetric pulse profile and longer pulse duration for 1250 and 1275 nm center wavelengths when tuning the output from the NOPA laser. Full characterization and correction for dispersion to allow the shortest pulse at the sample is especially important for 3P microscopy where the fluorescent signal, I_s , is highly dependent on the pulse duration, τ , by the relation, $I_s \sim \frac{1}{\tau}$.²⁴

4.4 SBR Dependence on Pulse Duration

When tuning the wavelength from 1225 to 1360 nm, the excitation of tdTomato changes from a predominately 2P process, to a mixture of 2P/3P, to a 3P process. Interestingly, when there is a mixture of 2P/3P, the SBR shows a strong dependence on the pulse duration ($\sim 1/\tau$). However, for a fully 2P process or fully 3P process where the background is above the detector noise level, there is a weaker dependence of SBR on pulse duration (see Fig. S4 in Ref. 38 and Fig. S5 in Ref. 24).

For mixed 2P/3P excitation, we can approximate the SBR as¹⁷

$$\text{SBR}_{\text{Total}} \sim \text{SBR}_{2\text{P}} \left(1 + \frac{S_{3\text{P}}}{S_{2\text{P}}} \right).$$

The ratio of 3P signal versus 2P is affected by both the pulse duration (FWHM), τ , and the second- and third-order temporal coherence of the pulse ($g_p^{(2)}$ and $g_p^{(3)}$)¹⁷ in the form, which is stated as

$$\frac{S_{3P}}{S_{2P}} = \frac{3.5\pi(\text{NA})^2 \sigma_3 \langle P(t) \rangle}{12 \sigma_2 f \lambda^2} \left(\frac{g_p^{(3)}}{g_p^{(2)} \tau} \right),$$

where σ_2 and σ_3 are the 2P and 3P cross-sections, respectively, $\langle P(t) \rangle$ is the time-averaged excitation photon flux (photons/s), NA is the numerical aperture, f is the laser repetition rate, and λ is the excitation wavelength. Therefore, we expect a lower SBR at 1250 and 1275 nm due to the longer pulse durations and asymmetric pulse shapes at those wavelengths.

As a further illustration, we theoretically calculated the $\text{SBR}_{\text{Total}}/\text{SBR}_{2P}$ for tdTomato as a function of pulse duration using the 2P and 3P cross-sections measured at 1260 nm excitation and the following parameters: 2 nJ pulse energy, 1 MHz repetition rate, 0.8 NA, $g_p^{(2)} = 0.587$, and $g_p^{(3)} = 0.413$ for hyperbolic-secant-squared pulse. Results are shown in Fig. S6 in the [Supplemental Materials](#). As can be seen, the value for a 100 fs pulse is 53.7% lower than for a 50 fs pulse. The 3P excitation cross-section versus wavelength for mScarlet has not been measured so it is uncertain over which wavelength range the 2P/3P transition occurs.

4.5 Advantages of Single Wavelength Dual-Color 3P Imaging

Optical engineering of microscopes capable of simultaneous 1300- and 1700-nm 3P excitation presents multiple difficulties. Current commercially available optical elements (e.g., Pockels cells) are not commonly tested in the 1700-nm range, and achieving adequate transmission of the excitation light out the objective may require additional purchases and/or custom modifications. Additionally, 1700-nm light requires independent pulse dispersion optimization, and for simultaneous imaging, multiple excitation sources must be mixed and aligned for each imaging session. The results presented here suggest that for certain applications of structural dual-color 3P excitation, specific fluorophore combinations can be used to exploit the enhanced 3P cross-sections of RFPs in the 1300-nm range without the need for a second 1700-nm excitation path. Still, the development of simultaneous 1300-/1700-nm systems will be important for future studies using dynamic optochemical indicators and/or optical stimulation deep in the brain. Furthermore, it was reported that, unlike tdTomato and mScarlet, mCherry exhibits a sevenfold decreased 3P cross-section in the 1300-nm range compared to 1650 nm,¹⁷ and thus may require a 1300-/1700-nm system to be optimally employed as a fluorescent reporter for dual-color 3P imaging.

4.6 Scattering and Absorption in the 1300- to 1400-nm Range

The EAL for 3P microscopy is defined as the depth at which the unscattered excitation light is reduced by $1/e^3$. In the mouse brain, both 2P and 3P EAL are determined by a combination of scattering and water absorption. 2P and 3P EALs in different regions of the mouse brain have been characterized extensively, both *in vivo* and *in silico*.^{12,14,20,23,24,33,39,40} Therefore, considerations such as the scattering and water absorption, as well as the output power from current NOPA configurations should be taken into account for dual-color 3P imaging with a single excitation source in the 1300-nm range. In this study, we did not achieve sufficient output power at 1 MHz and wavelengths greater than 1340 nm to allow for practical deep *in vivo* imaging, however, excitation in the 1325- to 1340-nm range provided exceptional SBR for both tdTomato and mScarlet. Because water absorption increases exponentially between 1340 and 1400 nm, our results are encouraging in that a narrow excitation window (1320 to 1340 nm) may be used to excite a broad range of green and red fluorescent reporter combinations with a single wavelength. Future work includes empirically testing a suite of fluorescent reporters for use in multi-color 3P experiments, using emission path engineering to increase the number of detection channels, and defining 3P activation properties of opsins and other dynamic indicators.

Disclosures

K.K. is a co-founder and part-owner of 3i. The other authors declare no competing financial interests.

Acknowledgments

We thank Dr. Chris Xu for his invaluable advice in setting up the 3P microscope at the University of Colorado Anschutz Medical Campus; Dr. Karl Deisseroth for providing us with the AAV8-hSyn-mScarlet-WPRE virus; Anthony Chavez for technical and veterinary assistance; Andrew Scallon and the CU Anschutz Optogenetics and Neural Engineering Core (P30NS048154) for 3D printing and stage design; members of the Hughes and Welle labs for discussions. M.A.T. is supported by the National Institutes of Health NINDS (F31NS120540). Funding was provided by NINDS NS115975, the University of Colorado Department of Cell and Developmental Biology Pilot Grant, the Whitehall Foundation, and the National Multiple Sclerosis Society (RG-1701–26733) to E.G.H. Funding was provided by the National Institutes of Health NINDS (R01 NS118188 and UF1 NS116241) and the National Science Foundation (BCS-1926676) to E.A.G. and D.R. E.G.H., E.A.G., and M.A.T. conceived the project. G.L.F. and E.A.G. built the microscope. M.A.T. conducted experiments and generated Figs. 1(a)–3 and Figs. S1a, S3, S4, and S5 in the [Supplemental Materials](#). G.L.F. designed and contributed Figs. 1(b) and Figs. S1b and S2 in the [Supplemental Materials](#). M.E.S. analyzed data in Figs. 2 and 3 and Figs. S3 and S5 in the [Supplemental Materials](#). E.A.G. conducted the modeling for Figure S6 in the [Supplemental Materials](#). B.N.O. and K.K. developed the software and helped with microscope setup. E.G.H., E.A.G., and D.R. supervised all experiments. M.A.T. and E.G.H. wrote the manuscript with input and editing from all other authors.

Code, Data, and Materials Availability

All data that support the findings, tools, and reagents will be shared on an unrestricted basis; requests should be directed to the corresponding authors.

References

1. E. E. Hoover and J. A. Squier, “Advances in multiphoton microscopy technology,” *Nat. Photonics* **7**(2), 93–101 (2013).
2. F. Helmchen and W. Denk, “Deep tissue two-photon microscopy,” *Nat. Methods* **2**(12), 932–940 (2005).
3. T. Wang and C. Xu, “Three-photon neuronal imaging in deep mouse brain,” *Optica* **7**(8), 947 (2020).
4. M. A. Gaffield et al., “Inhibition gates supralinear Ca²⁺ signaling in Purkinje cell dendrites during practiced movements,” *eLife* **7**, e36246 (2018).
5. S. Han, W. Yang, and R. Yuste, “Two-color volumetric imaging of neuronal activity of cortical columns,” *Cell Rep.* **27**(7), 2229–2240.e4 (2019).
6. H. Kawano et al., “Two-photon dual-color imaging using fluorescent proteins,” *Nat. Methods* **5**(5), 373–374 (2008).
7. C. Xu and W. W. Webb, “Measurement of two-photon excitation cross sections of molecular fluorophores with data from 690 to 1050 nm,” *J. Opt. Soc. Am. B* **13**(3), 481 (1996).
8. C. Ricard et al., “Two-photon probes for *in vivo* multicolor microscopy of the structure and signals of brain cells,” *Brain Struct. Funct.* **223**(7), 3011–3043 (2018).
9. M. Drobizhev et al., “Two-photon absorption properties of fluorescent proteins,” *Nat. Methods* **8**(5), 393–399 (2011).
10. H. Dana et al., “Sensitive red protein calcium indicators for imaging neural activity,” *eLife* **5**, e12727 (2016).
11. E. G. Hughes et al., “Myelin remodeling through experience-dependent oligodendrogenesis in the adult somatosensory cortex,” *Nat. Neurosci.* **21**(5), 696–706 (2018).

12. N. G. Horton et al., “In vivo three-photon microscopy of subcortical structures within an intact mouse brain,” *Nat. Photonics* **7**(3), 205–209 (2013).
13. D. G. Ouzounov et al., “In vivo three-photon imaging of activity of GCaMP6-labeled neurons deep in intact mouse brain,” *Nat. Methods* **14**(4), 388–390 (2017).
14. T. Wang et al., “Quantitative analysis of 1300-nm three-photon calcium imaging in the mouse brain,” *eLife* **9**, e53205 (2020).
15. K. Guesmi et al., “Dual-color deep-tissue three-photon microscopy with a multiband infrared laser,” *Light Sci. Appl.* **7**(1), 12 (2018).
16. M. Yildirim et al., “Functional imaging of visual cortical layers and subplate in awake mice with optimized three-photon microscopy,” *Nat. Commun.* **10**(1), 177 (2019).
17. Y. Hontani, F. Xia, and C. Xu, “Multicolor three-photon fluorescence imaging with single-wavelength excitation deep in mouse brain,” *Sci. Adv.* **7**(12), eabf3531 (2021).
18. J. H. Marshel et al., “Cortical layer-specific critical dynamics triggering perception,” *Science* **365**(6453), eaaw5202 (2019).
19. C. M. Bacmeister et al., “Motor learning promotes remyelination via new and surviving oligodendrocytes,” *Nat. Neurosci.* **23**(7), 819–831 (2020).
20. K. Podgorski and G. Ranganathan, “Brain heating induced by near-infrared lasers during multiphoton microscopy,” *J. Neurophysiol.* **116**(3), 1012–1023 (2016).
21. P. Thévenaz, U.E. Ruttimann, and M. Unser, “A pyramid approach to subpixel registration based on intensity,” *IEEE Trans. Image Process.* **7**(1), 27–41 (1998).
22. C. A. Schneider, W. S. Rasband, and K. W. Eliceiri, “NIH image to ImageJ: 25 years of image analysis,” *Nat. Methods* **9**(7), 671–675 (2012).
23. M. Wang et al., “Comparing the effective attenuation lengths for long wavelength *in vivo* imaging of the mouse brain,” *Biomed. Opt. Express* **9**(8), 3534–3543 (2018).
24. P. Theer and W. Denk, “On the fundamental imaging-depth limit in two-photon microscopy,” *J. Opt. Soc. Am. A* **23**(12), 3139–3149 (2006).
25. R. Trebino et al., “Measuring ultrashort laser pulses in the time-frequency domain using frequency-resolved optical gating,” *Rev. Sci. Instrum.* **68**(9), 3277–3295 (1997).
26. D. J. Kane, “Recent progress toward real-time measurement of ultrashort laser pulses,” *IEEE J. Quantum Electron.* **35**(4), 421–431 (1999).
27. D. M. Farinella et al., “Improving laser standards for three-photon microscopy,” *Neurophotonics* **8**(1), 015009 (2021).
28. T. J. Lambert, “FPbase: a community-editable fluorescent protein database,” *Nat. Methods* **16**, 277–278 (2019).
29. M. Drobizhev et al., “Local electric field controls fluorescence quantum yield of red and far-red fluorescent proteins,” *Front. Mol. Biosci.* **8**, 633217 (2021).
30. T. W. McCulloch et al., “Comparing the performance of mScarlet-1, mRuby3, and mCherry as FRET acceptors for mNeonGreen,” *PLoS One* **15**(2), e0219886 (2020).
31. V. Dunsing et al., “Optimal fluorescent protein tags for quantifying protein oligomerization in living cells,” *Sci. Rep.* **8**(1), 10634 (2018).
32. N. C. Shaner et al., “Improved monomeric red, orange and yellow fluorescent proteins derived from *Discosoma* sp. red fluorescent protein,” *Nat. Biotechnol.* **22**(12), 1567–1572 (2004).
33. C. J. Liu et al., “Three-photon imaging of synthetic dyes in deep layers of the neocortex,” *Sci. Rep.* **10**(1), 16351 (2020).
34. D. S. Bindels et al., “mScarlet: a bright monomeric red fluorescent protein for cellular imaging,” *Nat. Methods* **14**(1), 53–56 (2017).
35. L. Kou et al., “Refractive indices of water and ice in the 0.65-to 2.5- μm spectral range,” *Appl. Opt.* **32**(19), 3531–354 (1993).
36. J. Paye et al., “Measurement of the amplitude and phase of ultrashort light pulses from spectrally resolved autocorrelation,” *Opt. Lett.* **18**(22), 1946–1948 (1993).
37. R. Trebino and D. J. Kane, “Using phase retrieval to measure the intensity and phase of ultrashort pulses: frequency-resolved optical gating,” *J. Opt. Soc. Am. A* **10**(5), 1101–1111 (1993).
38. N. Akbari et al., “Imaging deeper than the transport mean free path with multiphoton microscopy,” *Biomed. Opt. Express* **13**(1), 452–463 (2022).

39. M. Wang et al., “In vivo three-photon imaging of deep cerebellum,” *Proc. SPIE* **10498**, 1049816 (2018).
40. C. Xu et al., “Multiphoton fluorescence excitation: new spectral windows for biological nonlinear microscopy,” *Proc. Natl. Acad. Sci. U.S.A.* **93**(20), 10763–10768 (1996).

Michael A. Thornton is a PhD candidate in the Neuroscience Graduate Program at the University of Colorado, Anschutz Medical Campus. He received his BS degree in psychobiology and his MS degree in physiological science from the University of California, Los Angeles before joining Dr. Ethan Hughes’ Lab for his PhD research.

Karl Kilborn is a co-founder and co-president of 3i. He received his PhD in computer science at the University of California, Irvine, where he studied computational neuroscience. His current research focus at 3i is developing new tools incorporating multiphoton imaging, computer-generated holography, and fluorescence lifetime.

Emily A. Gibson is an associate professor in the Department of Bioengineering, University of Colorado Anschutz Medical Campus, with a joint appointment in the Department of Physiology and Biophysics and Neuroscience Program. She received her PhD in physics from the University of Colorado at Boulder, with a specialization in nonlinear optics. Her research focus is the development of optical technologies for clinical and biomedical research applications. She has expertise in microscopy and spectroscopy techniques for measurement of biological samples from cellular to *in vivo* models.

Ethan G. Hughes is an assistant professor in the Cell and Developmental Biology Department at the University of Colorado School of Medicine. He received his BS degree in biology with special honors from George Washington University in 2003 and his PhD in the Laboratory of Rita Balice-Gordon at the University of Pennsylvania in 2009. He was a postdoctoral fellow under the mentorship of Dwight Bergles at Johns Hopkins University.

Biographies of the other authors are not available.